

# Sasaki Metric for Spline Models of Manifold-Valued Trajectories

Esfandiar Nava-Yazdani<sup>a,\*</sup>, Felix Ambellan<sup>a,b</sup>, Martin Hanik<sup>a,b</sup>, Christoph von  
Tycowicz<sup>b</sup>

<sup>a</sup>*Zuse Institute Berlin, Germany*

<sup>b</sup>*Freie Universität Berlin, Germany*

---

## Abstract

We propose a generic spatiotemporal framework to analyze manifold-valued measurements, which allows for employing an intrinsic and computationally efficient Riemannian hierarchical model. Particularly, utilizing regression, we represent discrete trajectories in a Riemannian manifold by composite Bézier splines, propose a natural metric induced by the Sasaki metric to compare the trajectories, and estimate average trajectories as group-wise trends. We evaluate our framework in comparison to state-of-the-art methods within qualitative and quantitative experiments on hurricane tracks. Notably, our results demonstrate the superiority of spline-based approaches for an intensity classification of the tracks.

*Keywords:* Riemannian regression, Sasaki metric, Hurricane, Manifold-valued trajectory, Bézier spline, Tangent bundle, Functional data analysis

---

## 1. Introduction

A wide range of applications in many areas including morphology, action recognition and computer vision requires longitudinal study of manifold-valued data. Approaches relying on the Euclidean structure of the embedding space or local coordinates do not correctly incorporate the inherent underlying geometry. Particularly, representing the geometry of trajectories in Euclidean spaces undermines the ability to represent natural variability in populations. The need for geometry-aware approaches has led to an increasing number of works on comparison of manifold-valued trajectories via Riemannian metrics (Muralidharan and Fletcher, 2012; Le Brigant et al., 2015; Schiratti et al., 2015; Bauer et al., 2017; Debavelaere et al., 2020; Dai et al., 2021; Bauer et al., 2021; Shao et al., 2022; Nava-Yazdani et al., 2022b; Hanik et al., 2022).

---

\*Corresponding author

*Email addresses:* [navayazdani@zib.de](mailto:navayazdani@zib.de) (Esfandiar Nava-Yazdani), [ambellan@zib.de](mailto:ambellan@zib.de) (Felix Ambellan), [hanik@zib.de](mailto:hanik@zib.de) (Martin Hanik), [vontycowicz@zib.de](mailto:vontycowicz@zib.de) (Christoph von Tycowicz)

A Riemannian framework for statistics and analysis in the space of trajectories is appealing because it provides a rich structure for which powerful tools are already available. Since the space of general trajectories is infinite-dimensional, it is highly complex. Particularly for numerical treatments, it is thus desirable to replace it with an adequate finite dimensional space. A natural and powerful method towards this goal is to represent the trajectories by finitely parametrized curves via regression, which is a ubiquitous tool in various application fields. This includes piece-wise geodesic, kernel, polynomial, logistic (see (Fishbaugh et al., 2012) and the references therein), and Fourier regression (Suparti et al., 2019).

The most common method for regression on a manifold is geodesic regression (cf. (Machado and Silva Leite, 2007; Niethammer et al., 2011; Fletcher, 2013; Nava-Yazdani et al., 2020, 2022b)), which is the counterpart of linear regression in Euclidean space. Often, the relation between the variables is highly complex, and therefore geodesic regression can prove to be inadequate for model selection toward a best-fitting curve. In such cases, it is necessary to resort to a more flexible model for regression. For this purpose, a generalization that relies on intrinsic polynomials in Riemannian manifolds was proposed in (Hinkle et al., 2014). However, due to their flexibility and effective evaluation in terms of simple iterative algorithms for a constructive approach, Bézier splines (Popiel and Noakes, 2007; Gousenbourger et al., 2019) are more adequate as best-fitting curves for regression. Note that, inconsistencies are minimized by considering best-fitting smooth curves.

In this work, we employ the spline regression approach that was recently proposed in (Hanik et al., 2020) and (Hanik et al., 2022) to approximate trajectories. We show that the resulting space of Bézier splines is finite-dimensional and that it can be endowed with a natural Riemannian metric that stems from the famous Sasaki metric. Utilizing this structure, one can intrinsically employ principal component analysis and, particularly, compute group trends as average trajectories; the latter establishes a generic hierarchical model (cf. (Muralidharan and Fletcher, 2012; Nava-Yazdani et al., 2022b; Hanik et al., 2022)).

We verify the virtue of the proposed framework by applying it to data on the 2010-2021 Atlantic hurricane tracks. Also referred to as tropical cyclones, hurricanes belong to the most destructive natural disasters. They can have an enormous impact on environment, economy, and human life (Weinkle et al., 2018). We compare our approach to state-of-the-art methods regarding an intensity classification for the tracks. This comparison substantiates the advantages of the proposed approach. The code implementing our method is publicly available in `morphomatics` (Ambellan et al., 2021) v3.0 and the experiments in <https://github.com/morphomatics/GeometricHurricaneAnalysis>.

This paper is organized as follows. In the next section, we describe the mathematical framework and proposed hierarchical model. Therein, we present the spline regression and the Sasaki metric, which will be used to compare the splines representing the trajectories. Section 3 presents the application of our approach to hurricane tracks. Therein, we present results for the intrinsic hierarchical analysis of the hurricane tracks as well as our classification experiment and a discussion of the numerical outcome.

## 2. Mathematical Framework and Method

### 2.1. Background

We start by summarizing important facts on the geometry of the tangent bundle. For more background information see, e.g., (do Carmo, 1992). Let  $(M, g)$  be a  $n$ -dimensional smooth<sup>1</sup> Riemannian manifold and  $TM$  its tangent bundle with bundle projection  $\pi : TM \rightarrow M$ ,  $(p, v) \mapsto p$ . We denote the tangent space at  $p \in M$  by  $T_pM$  and the restriction of  $g$  to  $T_pM$  by  $g_p$ . We always assume that maps are smooth.

Being a  $2n$ -dimensional manifold itself, the natural Riemannian metric of  $TM$  is the Sasaki metric. For the definition of the latter, recall that the tangent bundle  $TTM$  of  $TM$  is the direct sum of a vertical subbundle  $VTM$  (the kernel of the derivative  $d\pi$  of  $\pi$ ) and a horizontal subbundle  $HTM$  determined by the Levi-Civita connection  $\nabla$  of  $M$  as vectors tangent to parallel vector fields, and both have rank  $n$ . Intuitively, horizontal vectors are directions in which only the footpoint changes, whereas the latter is constant in vertical directions. The Sasaki metric (Sasaki, 1962) is the unique Riemannian metric on  $TM$  with the following properties:

- The bundle projection  $\pi$  is a Riemannian submersion, i.e.  $\pi$  has maximal rank and  $d\pi$  preserves lengths of horizontal vectors.
- For any  $p \in M$ , the restriction of  $\tilde{g}$  to the tangent space  $T_pM \subset TM$  coincides with  $g_p$ .
- Let  $u$  be a *parallel* vector field along a curve  $q : (-\varepsilon, \varepsilon) \rightarrow M$ . Define  $\zeta = (-\varepsilon, \varepsilon) \rightarrow TM$ ,  $t \mapsto (q(t), u(t))$ . Let further  $p = q(0)$  lie on  $q$  and  $v : (-\varepsilon, \varepsilon) \rightarrow T_pM$  such that  $u(0) = v(0)$ . Define  $\eta : (-\varepsilon, \varepsilon) \rightarrow TM$ ,  $t \mapsto (p, v(t))$ . Then  $\dot{\zeta}(0) := \frac{d}{dt}\zeta(0) \in H_{(p, u(0))}TM$  and  $\dot{\eta}(0) = \frac{d}{dt}\eta(0) \in V_{(p, u(0))}TM$  are orthogonal.

It follows that horizontal and vertical vectors are orthogonal.

Let  $(p, u) \in TM$ . Because  $H_{(p, u)}TM$  and  $V_{(p, u)}TM$  are  $n$ -dimensional vector spaces, both can be identified with  $T_pM$ ; in other words, we can view an element of  $T_{(p, u)}TM$  as a tuple  $(v, w) \in (T_pM)^2$ . As horizontal and vertical components are orthogonal, the Sasaki metric between  $(v_1, w_1), (v_2, w_2) \in T_{(p, u)}TM$  then reads

$$\tilde{g}_{(p, u)}((v_1, w_1), (v_2, w_2)) = g_p(v_1, v_2) + g_p(w_1, w_2). \quad (1)$$

Geodesics of the Sasaki metric can be characterized in terms of geometric features of the underlying space. Let  $\eta = (q, u) : (-\varepsilon, \varepsilon) \rightarrow TM$  be a curve in  $TM$  and  $\dot{\eta} = (v, w)$ . Denoting the Riemannian curvature tensor of  $M$  by  $R$ ,  $\eta$  is a geodesic if (and only if) the coupled system

$$\begin{aligned} \nabla_v v &= -R(u, w)v, \\ \nabla_v w &= 0 \end{aligned}$$

---

<sup>1</sup>In this work, “smooth” stands for “infinitely differentiable.”

holds. Intuitively, the above equations say that the footpoint curve  $q$  bends according to the curvature of  $M$ , while the vector component  $u$  changes at a constant rate.

Further properties of  $(TM, \tilde{g})$ , e.g. its curvature tensor and Levi-Civita connection, can be found in (Gudmundsson and Kappos, 2002).

## 2.2. Bézier Splines

Let  $U$  denote a normal convex (sometimes also called totally normal) neighborhood in  $M$ . Thus, the diameter of  $U$  is less than the injectivity radius of  $M$  and the Riemannian logarithm  $\log$  is defined on the whole of  $U$ . In particular, for any  $p, q \in U$  there is a unique geodesic from  $p$  to  $q$  that never leaves  $U$  given by

$$\gamma(t; p, q) := \exp_p(t \log_p q), \quad 0 \leq t \leq 1.$$

Requiring that the data lies in  $U$  ensures well-posedness of our construction. If  $M$  is a Hadamard manifold, then we can simply set  $U = M$ . For points  $p_0, \dots, p_k \in U$ , we set the following.

**Definition 2.1** (De Casteljau's Algorithm on Manifolds).

$$\begin{aligned} \beta_i^0(t) &:= p_i, \quad i = 0, \dots, k-r, \\ \beta_i^r(t) &:= \gamma(t; \beta_i^{r-1}(t), \beta_{i+1}^{r-1}(t)), \quad r = 1, \dots, k, \quad 0 \leq t \leq 1. \end{aligned}$$

We call  $\beta := \beta_0^k$  *Bézier curve of degree  $k$  with control points  $p_0, \dots, p_k$* . For more details on them and some applications, we refer to (Popiel and Noakes, 2007) and (Nava-Yazdani and Polthier, 2013). Notation-wise, whenever we want to make the dependency on the control points clear, we write  $\beta(t; p_0, \dots, p_k)$  instead of  $\beta(t)$  for the value of  $\beta$  at  $t$ .

This work is centered around cubic Bézier curves, i.e. we consider the case  $k = 3$ . Then, control points and velocities at endpoints satisfy

$$\begin{aligned} p_1 &= \exp_{p_0} \left( \frac{1}{3} \dot{\beta}(0) \right), \\ p_2 &= \exp_{p_3} \left( -\frac{1}{3} \dot{\beta}(1) \right). \end{aligned} \tag{2}$$

or equivalently

$$\begin{aligned} \dot{\beta}(0) &= 3 \log_{p_0} p_1, \\ \dot{\beta}(1) &= -3 \log_{p_3} p_2. \end{aligned} \tag{3}$$

These properties can be exploited to define differentiable (or composite) Bézier splines (Gousenbourger et al., 2019; Hanik et al., 2020). In the following, we explain this construction. For  $i = 0, \dots, L-1$ , let  $(p_0^{(i)}, p_1^{(i)}, p_2^{(i)}, p_3^{(i)})$  be the control points of  $L \geq 2$  cubic Bézier curves  $\beta^{(0)}, \dots, \beta^{(L-1)}$  such that

$$p_3^{(i)} = p_0^{(i+1)} \quad \text{and} \quad \gamma(2; p_2^{(i)}, p_3^{(i)}) = p_1^{(i+1)} \tag{4}$$

for all  $i = 0, \dots, L - 2$ . The *cubic Bézier spline*  $B$  with control points

$$\left( p_0^{(i)}, p_1^{(i)}, p_2^{(i)}, p_3^{(i)} \right)_{i=0, \dots, L-1}$$

is then defined by

$$B(t) := \begin{cases} \beta^{(0)} \left( t; p_0^{(0)}, p_1^{(0)}, p_2^{(0)}, p_3^{(0)} \right), & t \in [0, 1], \\ \beta^{(i)} \left( t - i; p_0^{(i)}, p_1^{(i)}, p_2^{(i)}, p_3^{(i)} \right), & t \in (i, i + 1], \quad i = 1, \dots, L - 1. \end{cases}$$

Note that it is  $C^1$  by construction. We also consider Bézier curves as splines with a single segment (the  $L = 1$  case).

### 2.3. The Bézierfold

In the following, we present a natural Riemannian metric for the splines. To this end, we introduce the following.

**Definition 2.2** (Bézierfold of cubic splines). *Let  $U$  be a normal convex neighborhood of an  $n$ -dimensional Riemannian manifold  $M$ . We define the Bézierfold  $\mathcal{B}_3^L(U)$  of cubic splines by*

$$\mathcal{B}_3^L(U) := \{ B : [0, L] \rightarrow U \mid B \text{ is a cubic Bézier spline with } L \text{ segments} \}.$$

Now, fix  $L$  and  $U$ . To simplify notation, we write  $\mathcal{B}$  for  $\mathcal{B}_3^L(U)$ . As remarked (but not proven) in (Hanik et al., 2022),  $\mathcal{B}$  can be given the structure of a smooth manifold when splines are identified with a suitable subset of their control points. In the following, we will rigorously prove this assertion, albeit using a different identification map. The advantage of the latter is that it immediately allows us to define our novel metric on  $\mathcal{B}$ .

**Theorem 1.** *The Bézierfold  $\mathcal{B}$  can be given the structure of a smooth  $(2L + 2)n$ -dimensional manifold.*

*Proof.* We define the map

$$\begin{aligned} F : \mathcal{B} &\rightarrow (TU)^{L+1}, \\ B &\mapsto \left( (B(0), \dot{B}(0)/3), \dots, (B(L), \dot{B}(L)/3) \right). \end{aligned} \tag{5}$$

Equation (3) yields

$$F(B) = \left( \left( p_0^{(0)}, \log_{p_0^{(0)}}(p_1^{(0)}) \right), \dots, \left( p_0^{(L-1)}, \log_{p_0^{(L-1)}}(p_1^{(L-1)}) \right), \right. \\ \left. \left( p_3^{(L-1)}, -\log_{p_3^{(L-1)}}(p_2^{(L-1)}) \right) \right).$$

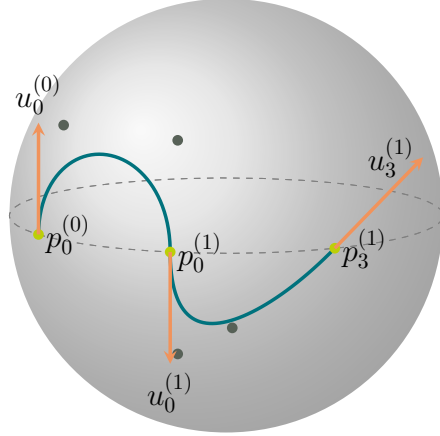


Figure 1: Cubic Bézier spline with two segments on the 2-dimensional sphere  $S^2$ . Footpoints are shown in green while vectors are in orange. Here,  $u_0^{(i)} := \log_{p_0^{(i)}}(p_1^{(i)})$ ,  $u_0^{(1)} := \log_{p_0^{(1)}}(p_1^{(1)})$ , and  $u_3^{(1)} := -\log_{p_3^{(1)}}(p_2^{(1)})$ . Control points that are not used in the representation are gray.

Crucially,  $F$  is bijective: It follows from (2) and (4) that  $F^{-1}$  is the map that assigns to each element

$$((p_0, u_0), (p_1, u_1), \dots, (p_L, u_L)) \in (TU)^{L+1}$$

the Bézier spline with control points

$$(p_0^{(i)}, p_1^{(i)}, p_2^{(i)}, p_3^{(i)}) = (p_i, \exp_{p_i}(u_i), \exp_{p_{i+1}}(-u_{i+1}), p_{i+1}), \quad i = 0, \dots, L-1. \quad (6)$$

The manifold structure is now obtained by pulling back (Postnikov, 2013, Ch. 30 § 9) the (product) structure of  $(TU)^{L+1}$  along  $F$ . We thus obtain the induced topology. Furthermore, if  $V \subseteq (TU)^{L+1}$  and  $\phi : V \rightarrow \mathbb{R}^{(2L+2)n}$  form a chart  $(V, \phi)$  of  $(TU)^{L+1}$ , then  $(F^{-1}(V), \phi \circ F)$  is a chart of  $\mathcal{B}$ . The set of all charts that are constructed in this way constitutes the maximal (smooth) atlas of  $\mathcal{B}$ .  $\square$

Note that, with the above construction,  $F$  is a diffeomorphism. In Fig. 1, we visualize a Bézier spline with 2 segments on  $S^2$  together with the 3 elements of  $TS^2$  to which it is mapped by  $F$ .

#### 2.4. Sasaki Metric for the Bézierfold

We can now use  $F$  to pull the (product) Sasaki metric back to the Bézierfold. To this end, we first investigate how the  $F^{-1}$  characterizes the tangent spaces of the Bézierfold. Therefore, we use the following notation. If  $f : M \rightarrow N$  is a map between manifolds  $M$  and  $N$ , we denote the derivative of  $f$  at  $p$  in direction  $u \in T_p M$  by  $d_p f(u)$ . When we differentiate the exponential  $\exp_p(u)$  w.r.t. the footpoint at  $p$ , we write  $(d_p \exp_{(\cdot)}(u))(v)$ .

Let  $B \in \mathcal{B}$ . Because of (6), there is  $((p_0, u_0), (p_1, u_1) \dots, (p_L, u_L)) \in (TU)^{L+1}$  such that the control points of  $B$  are given by

$$\left( p_i, \exp_{p_i}(u_i), \exp_{p_{i+1}}(-u_{i+1}), p_{i+1} \right)_{i=0, \dots, L-1}.$$

Since derivatives of diffeomorphisms are everywhere isomorphisms between tangent spaces, we find that  $T_B \mathcal{B}$  is the image of the tangent space  $T_{((p_0, u_0), \dots, (p_L, u_L))} (TU)^{L+1}$  under  $dF^{-1}$ . In the product structure, we can compute this image component-wise; therefore

$$T_B \mathcal{B} = \{X : [0, L] \rightarrow TM \mid \exists (v_0, w_0) \in T_{(p_0, u_0)} TM, \dots, (v_L, w_L) \in T_{(p_L, u_L)} TM : X = \sum_{i=0}^L d_{(p_i, u_i)} F^{-1}((v_i, w_i))\}. \quad (7)$$

Every element  $X \in T_B \mathcal{B}$  is thus a vector field along  $B$ . We say that it is induced by the vectors  $(v_0, w_0), \dots, (v_L, w_L) \in (TM)^2$ .

We now use  $B_j^{(i)}$  when we view only the  $j$ -th control point of the  $i$ -th segment of  $B$  as a variable, while all others (as well as  $t$ ) are fixed. Definition (5) then implies that, for each  $i \in \{0, \dots, L\}$ , the derivative of  $F^{-1}$  at  $(p_i, u_i)$  in direction  $(v_i, w_i)$  is

$$d_{(p_i, u_i)} F^{-1}((v_i, w_i)) = d_{(p_i, u_i)} B((v_i, w_i)).$$

For  $i \in \{1, \dots, L-1\}$  the chain rule then yields

$$\begin{aligned} d_{(p_i, u_i)} B((v_i, w_i)) &= d_{\exp_{p_i}(-u_i)} B_2^{(i-1)}(d_{-u_i} \exp_{p_i}(w_i)) \\ &\quad + d_{\exp_{p_i}(-u_i)} B_2^{(i-1)}(d_{p_i} \exp_{(\cdot)}(-u_i)(v_i)) \\ &\quad + d_{\exp_{p_i}(u_i)} B_1^{(i)}(d_{u_i} \exp_{p_i}(w_i)) \\ &\quad + d_{\exp_{p_i}(u_i)} B_1^{(i)}(d_{p_i} \exp_{(\cdot)}(u_i)(v_i)) + d_{p_i} B_0^{(i)}(v_i). \end{aligned} \quad (8)$$

For  $i = 0$  we get

$$\begin{aligned} d_{(p_0, u_0)} B((v_0, w_0)) &= d_{\exp_{p_0}(u_0)} B_1^{(0)}(d_{u_0} \exp_{p_0}(w_0)) \\ &\quad + d_{\exp_{p_0}(u_0)} B_1^{(0)}(d_{p_0} \exp_{(\cdot)}(u_0)(v_0)) + d_{p_0} B_0^{(0)}(v_0), \end{aligned} \quad (9)$$

and for  $i = L$

$$\begin{aligned} d_{(p_L, u_L)} B((v_L, w_L)) &= d_{\exp_{p_L}(-u_L)} B_2^{(L-1)}(d_{-u_L} \exp_{p_L}(w_L)) \\ &\quad + d_{\exp_{p_L}(-u_L)} B_2^{(L-1)}(d_{p_L} \exp_{(\cdot)}(-u_L)(v_L)) + d_{p_L} B_3^{(L-1)}(v_L). \end{aligned} \quad (10)$$

Note that we only take derivatives of single Bézier curves (the  $(i-1)$ -th and  $i$ -th segment) w.r.t. their control points. They are given by “concatenated” Jacobi

fields (Bergmann and Gousenbourger, 2018, Thm. 7). Furthermore, the derivatives of the exponential map are also Jacobi fields (Fletcher, 2013, Sec. 3.1). If  $M$  is a symmetric space, then (8), (9), (10), and thus elements of the tangent space (7) can be calculated explicitly (do Carmo, 1992, p. 121).

We endow  $T\mathcal{B}$  with the pullback  $g^*$  of the product Sasaki metric under  $F$ . To this end, let  $X, Y \in T\mathcal{B}$  and  $(v_0^X, w_0^X), \dots, (v_L^X, w_L^X) \in (TM)^2$  and  $(v_0^Y, w_0^Y), \dots, (v_L^Y, w_L^Y) \in (TM)^2$  be the vectors that induce them. Then, using (1), we obtain

$$\begin{aligned} g_B^*(X, Y) &:= \sum_{i=0}^L \tilde{g}_{(p_i, u_i)}((v_i^X, w_i^X), (v_i^Y, w_i^Y)) \\ &= \sum_{i=0}^L g_{p_i}(v_i^X, v_i^Y) + g_{p_i}(w_i^X, w_i^Y). \end{aligned}$$

Importantly, as  $\mathcal{B}$  and  $(TM)^{L+1}$  are now isometric (with isometry  $F$ ), we can always use the latter for computations, only transforming the results to  $\mathcal{B}$  (with  $F^{-1}$ ) as the final step. In particular, for the calculations in the next section, it is never necessary to evaluate a vector field along a Bézier curve explicitly; one only needs the vectors that induce it. This is one of the major advantages of our construction.

### 3. Application: Hurricane Tracks

Tropical cyclones, also referred to as hurricanes or typhoons, belong to the most supreme natural phenomena with enormous impact on environment, economy, and human life. The most common indicator for the intensity of a hurricane is its maximum sustained wind (maxwind), which classifies the storm into categories via the Saffir–Simpson hurricane wind scale. For instance,  $\text{maxwind} \geq 137$  knots corresponds to category 5. The maximal category over a track is called its category. Thus, the same applies to the maxwind.

High variability of tracks and out-most complexity of hurricanes has led to a huge number of works to classify, rationalize and predict them. We refer to (Rekabdarkolae et al., 2019) for a Bayesian function model, (Asif et al., 2018) for intensity estimation via machine learning and the overview of recent progress in tropical cyclone intensity forecasting (Cangialosi et al., 2020), and (Snaiki et al., 2020). We remark that many approaches are not intrinsic and use linear approximations. Notable exceptions are the works (Su et al., 2014, 2018) that employ an intrinsic Riemannian approach based on the squared root velocity framework, albeit only as illustrative examples and without consideration of maxwind.

#### 3.1. Dataset

We verify the effectiveness of the proposed framework by applying it to the 2010–2021 Atlantic hurricane tracks (total number 218) from the HURDAT 2 database provided by the U.S. National Oceanic and Atmospheric Administration publicly available on <https://www.nhc.noaa.gov/data/>. The data under consideration comprises



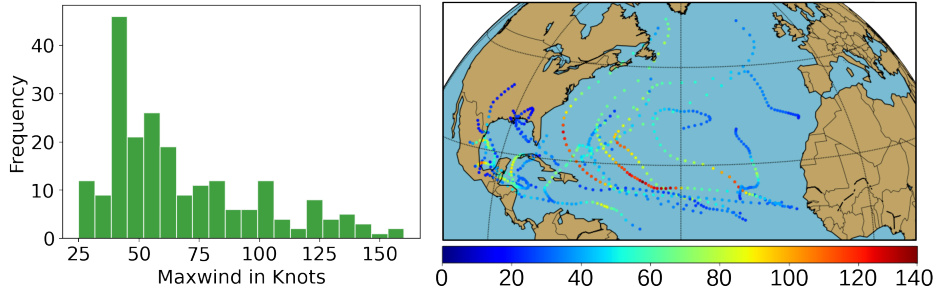


Figure 2: Maximum sustained wind (in knots): Color-coded for 2010 hurricane tracks (right) and histogram of maxima for all hurricanes (left).

measurements of latitude, longitude, and maxwind on a 6 hours base. Tracks are represented as discrete trajectories in  $S^2$ . The number of points constituting a track varies from 13 to 96 (on average 32). Fig. 2 illustrates this data set with a histogram of maximum sustained winds and a visualization of the 2010 hurricane tracks.

### 3.2. Spline Model

Before turning towards group-level analysis, we first derive spline representations for the trajectories. To this end, we consider the tracks to be observations of a manifold-valued random variable that depends on an explanatory scalar variable. Then the relationship of the hurricane location on (elapsed) time is modeled as a cubic spline  $B$ . The estimation of model parameters—the control points of the spline in our setting—is known as regression problem for which Riemannian generalizations are readily available. In particular, we employ the least-squares-based approach presented in (Hanik et al., 2020) that can be shown to provide maximum likelihood estimators for  $S^2$ -valued trajectories.

While we restrict our attention to cubic splines, we need to select the number of segments in order to obtain a fixed parametric model. We can adopt a qualitative selection strategy based on the goodness of fit as determined by the *coefficient of determination* denoted  $R^2$ . Specifically, let  $(q_1, t_1), \dots, (q_N, t_N) \in U \times [0, L]$  be the observations of a track at corresponding (normalized) times, then the geometric  $R^2$ -value (Fletcher, 2013) is given by

$$R^2 = 1 - \frac{\text{unexplained variance}}{\text{total variance}} = 1 - \frac{\frac{1}{N} \sum_i d(B(t_i), q_i)^2}{\min_{p \in U} \frac{1}{N} \sum_i d(p, q_i)^2}, \quad (11)$$

where the variances are determined by sums of squared geodesic distances  $d$  of the data to the model  $B$  respectively a single, best-fitting point in  $U$ . The latter is also referred to as Fréchet mean. As both variances are nonnegative, we have that  $R^2 \leq 1$  with equality if and only if the model  $B$  perfectly fits the data.

With the  $R^2$  statistic at hand, we perform regression analysis for the hurricane tracks employing single- as well as two-segment splines. Fig. 3 shows a histogram of  $R^2$  values for the estimated splines together with visualizations for two exemplary

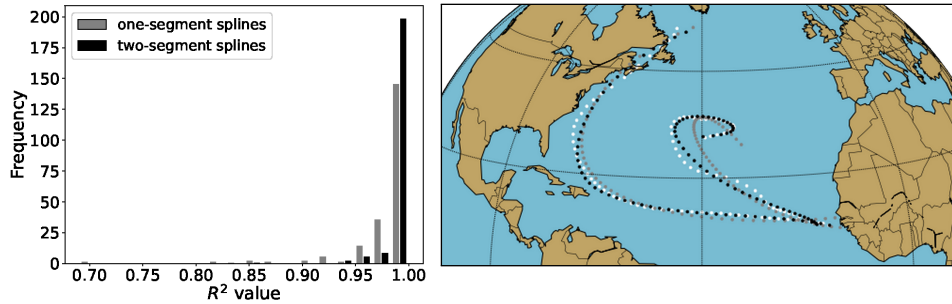


Figure 3: Left: Histogram of  $R^2$  values for the regressed cubic Bézier curves. Right: Two exemplary hurricane tracks (white) together with regressed one- and two-segment curves (gray/black) with  $R^2$  values of 0.995/0.998 and 0.916/0.993, respectively.

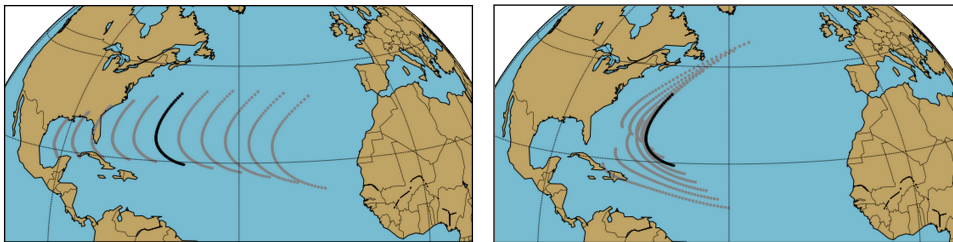


Figure 4: Two-segment spline Fréchet mean (black) and first two dominant modes of variation (gray; left: first mode, right: second mode) for hurricane tracks.

chosen hurricanes. While both spline representations expose a very high fidelity overall, the shift in distribution over  $R^2$  values toward 1 confirms a significant improvement of the two-segment model over single-segment ones. Given the upper bound of 1 for the  $R^2$  value, there is minor room for improvement by more complex models with three or more segments, thus rendering them inadequate according to the principle of parsimony (also known as Ockham’s razor).

### 3.3. Group-level Analysis

The presented geometric framework provides means to investigate hurricane tracks on a group level by studying their interrelations in terms of similarities and characteristic variations. In particular, the proposed metric induces a notion of variance and co-variances allowing to perform mean-variance analysis. To this end, we perform principal geodesic analysis (PGA) as proposed in (Fletcher et al., 2004). The estimated Fréchet mean together with the first and second dominant geodesic modes are visualized in Fig. 4.

We can further encode hurricane tracks with respect to the hierarchical basis determined by PGA, i.e. the dominant geodesic modes. By further omitting coordinates corresponding to the least dominant modes we obtain a low-dimensional representation that lends itself to visualization of the data. Henceforth, let  $\mathcal{M}$  denote the set

of absolutely continuous functions  $[0, 1] \rightarrow M$ . Physically motivated, we consider three groups: (i) tropical storms/depressions (category  $< 1$ ), (ii) hurricanes (category  $1 - 3$ ) with some to devastating damage, and (iii) major hurricanes (category  $> 3$ ) with catastrophic damage. Fig. 5 shows a scatter plot based on a two-dimensional encoding with respect to the proposed representation in Bézierfold  $\mathcal{B}$  in juxtaposition to treatment as elements of  $\mathcal{M}$  equipped with the  $L^2$  metric. In contrast to the latter, our representation shows an increased class separation particularly evident by the higher disparity between the group-wise means.

### 3.4. Intensity Classification

In the following, we investigate to which extent the (maximal) intensity of a hurricane can be inferred from its trajectory. Note that, while the dependency of maximum sustained wind on physical parameters and its spatiotemporal correlation is highly complex, in this experiment we are primarily interested in the discrimination ability of features derived from our proposed framework in comparison to those obtained from state-of-the-art. In particular, we will employ the hierarchical encoding provided by PGA (see also previous section) as features for classification. Due to the limited amount of available hurricane tracks and the strong disbalance with respect to hurricane categories, we opt for a support vector machine (SVM) as classifier. Thereby we condition the SVM model to differentiate between the three intensity classes described above. For all experiments we employ the implementation available in the `scikit-learn` v1.0 library using radial basis functions (kernel coefficient `gamma=0.7`) and regularization parameter `C=3`. We further perform balanced training by adapting class weights through a factor inversely proportional to class frequencies.

As a baseline, we compare our approach to the common  $L^2$  metric on  $\mathcal{M}$ . Thereby, to obtain a discrete counterpart  $\mathcal{M}^h$  of  $\mathcal{M}$  all hurricane tracks have been re-sampled to 32 points equidistantly spread (on the normalized time interval  $[0, 1]$ ). Additionally, we compare to two state-of-the-art approaches. On the one hand, we employ the square root velocity (SRV) framework from (Su et al., 2018) that provides an elastic metric on

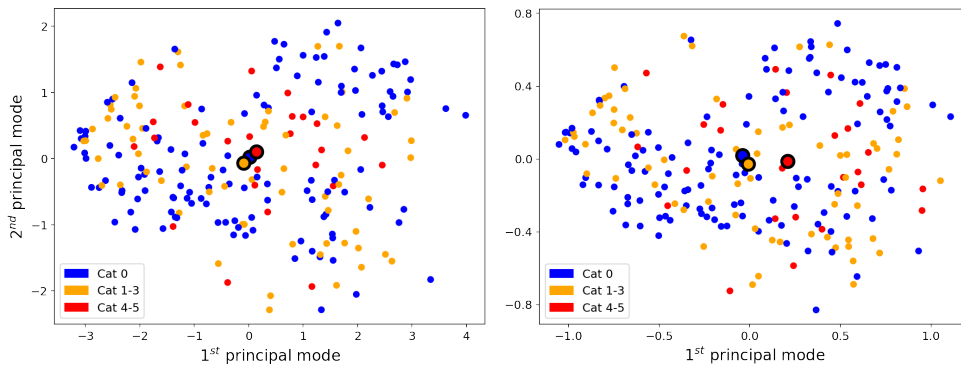


Figure 5: PGA loading plot of the first two principal geodesic modes for proposed (right) and  $L^2$  (left) metric. Group-wise means are highlighted with black boundaries.

$\mathcal{M}$ . On the other hand, we compare to the functionally-based metric for the intrinsic splines proposed in (Hanik et al., 2022), i.e. the  $L^2$  metric on  $\mathcal{B}$ .

For the evaluation of classification performance, we employ a balanced accuracy score given as the average of recall obtained in each class. Due to the limited cardinality of the hurricane data set, the partition into training and test data can emphasize or dampen the extent of problems like overfitting and selection bias. Therefore, we follow an extensive validation strategy in terms of 1000 random repetitions of 3-fold, stratified cross-validation. This allows for estimating the distribution of classification accuracies, which are shown in Fig. 6 for all methods under consideration. The results reveal significantly improved discrimination ability of spline-based representation with 61% and 59% accuracy for our proposed and the functional-based metric on average, respectively, as compared to  $\mathcal{M}$ -based ones with both  $\approx 49\%$  accuracy. These findings quantitatively confirm the superior performance for differentiation that was already qualitatively visible in the low-dimensional plots in Fig. 5. Note that the  $\dim(\mathcal{M}^h) = 64$  is considerably larger than  $\dim(\mathcal{B}) = 8$  leading to SVM with more degrees of freedom in the former case. Nevertheless, we would like to emphasize that the discrepancy in classification performance prevails also for dimensionality-reduced PGA encoding of curves in  $\mathcal{M}$ . This suggests that the increased discrimination performance can be attributed to the ability of regression schemes to suppress confounding factors such as variances in parameterization or noise.

### 3.5. Computational Performance

We conclude the experiments with an evaluation of the computational performance of algorithmic schemes for the analysis of manifold-valued splines. In particular, we compare our approach with the functional-based metric (Hanik et al., 2022) for the Bézierfold. Neither of these metrics provides explicit expressions for geodesics in  $\mathcal{B}$ . We, therefore, resort to iterative optimization based on variational time-discrete geodesics (Rumpf and Wirth, 2015). For the functional-based metric, we use the

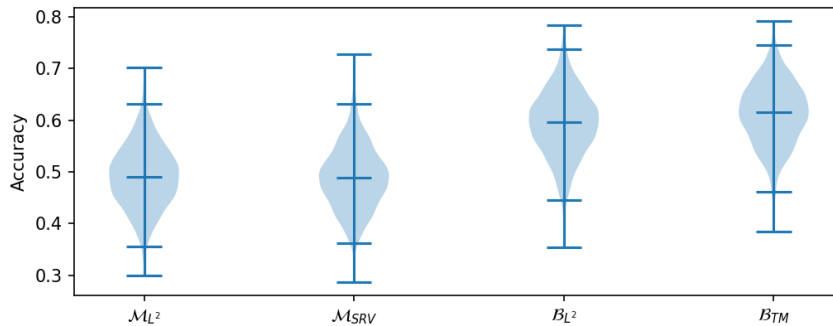


Figure 6: Distribution of classification accuracy for hurricanes treated as (from left to right) immersed curves in  $\mathcal{M}$  equipped the  $L^2$  and SRV-based elastic metric as well as splines in  $\mathcal{B}$  equipped with the  $L^2$  and the proposed metric.

implementation by Hanik et al. (2022) available via the `morphomatics` (Ambellan et al., 2021) v2.1.1 library. Based on this library, we also implemented time-discrete Sasaki geodesics as described in (Muralidharan and Fletcher, 2012; Nava-Yazdani et al., 2022a). For both metrics, we employ discrete 10-geodesics, i.e. intrinsic polygonal paths consisting of 10 segments. Furthermore, the functional-based metric is evaluated using a 4-point quadrature scheme.

In terms of complexity the mean-variance analysis, namely PGA, is the most costly part of our experiments as it requires iterative schemes with geodesic evaluations in each iteration. On a desktop computer (Intel i9-10920X CPU, NVIDIA GeForce RTX 3090 GPU), we obtain run times for PGA computation of 28s and 164s for the proposed and the functional-based metric, respectively. This considerable gap in performance can be attributed to the fact that the functional-based metric requires additional discretization of integrals along the trajectories involving geodesic distance on the base manifold— $S^2$  in our experiments. Furthermore, since explicit expressions for curvature estimation on  $S^2$  (and indeed many other practically relevant manifolds) are known, the Sasaki metric can be approximated very efficiently.

#### 4. Conclusion and Future Work

We presented a Riemannian framework for the comparison of manifold-valued trajectories. Therein, trajectories are represented by composite Bézier splines gained via regression. For the comparison of the trajectories, we proposed a natural extension of the Sasaki metric. This allows for estimating average trajectories representing group trends. We applied the proposed model to Atlantic hurricane tracks and presented experiments for an intensity classification of the tracks. Therein, we compared the proposed framework with those based on  $L^2$  as well as elastic metric, in which the results indicate clear advantages of our approach.

For future work, we intend to propose a generative model based on the introduced framework to enable online forecasting, employ statistical tests, and incorporate the main parameter determining the intensity of hurricanes, namely the Coriolis force and thermal effects, to improve the modeling. Moreover, we plan to apply our approach to further manifold-valued data and employ a geometry-aware recurrent neural network for classification.

#### 5. Acknowledgments

We are grateful for the HURDAT 2 database provided by the U.S. National Oceanic and Atmospheric Administration. This work was supported through the German Research Foundation (DFG) via individual funding (project ID 499571814) as well as under Germany’s Excellence Strategy – MATH+ : The Berlin Mathematics Research Center (EXC-2046/1 – project ID: 390685689), by the Bundesministerium für Bildung und Forschung (BMBF) through BIFOLD – The Berlin Institute for the Foundations of Learning and Data (ref. 01IS18025A and ref. 01IS18037A), and by the Bundesministerium für Wirtschaft und Klimaschutz through DAKI-FWS (01MK21009J).

## References

- Ambellan, F., Hanik, M., von Tycowicz, C., 2021. Morphomatics: Geometric morphometrics in non-euclidean shape spaces. doi:[10.12752/8544](https://doi.org/10.12752/8544). <https://morphomatics.github.io/>.
- Asif, A., Dawood, M., Jan, B., Khurshid, J., DeMaria, M., Minhas, F.A., 2018. Phurie: hurricane intensity estimation from infrared satellite imagery using machine learning. *Neural. Comput. Appl.* 32, 4821–4834. doi:[10.1007/s00521-018-3874-6](https://doi.org/10.1007/s00521-018-3874-6).
- Bauer, M., Bruveris, M., Harms, P., Møller-Andersen, J., 2017. A numerical framework for Sobolev metrics on the space of curves. *SIAM J. Imaging Sci.* 10, 47–73. doi:[10.1137/16M1066282](https://doi.org/10.1137/16M1066282).
- Bauer, M., Charon, N., Klassen, E., Le Brigant, A., 2021. Handbook of Mathematical Models and Algorithms in Computer Vision and Imaging: Mathematical Imaging and Vision. Springer. chapter Intrinsic Riemannian metrics on spaces of curves: theory and computation. pp. 1–35. doi:[10.1007/978-3-030-03009-4\\_87-1](https://doi.org/10.1007/978-3-030-03009-4_87-1).
- Bergmann, R., Gousenbourger, P.Y., 2018. A variational model for data fitting on manifolds by minimizing the acceleration of a Bézier curve. *Front. Appl. Math. Stat.* 4, 1–16. doi:[10.3389/fams.2018.00059](https://doi.org/10.3389/fams.2018.00059).
- Cangialosi, J.P., Blake, E., DeMaria, M., Penny, A., Latta, A., Rappaport, E., Tallapragada, V., 2020. Recent progress in tropical cyclone intensity forecasting at the national hurricane center. *Weather and Forecast.* 35, 1913–1922. doi:[10.1175/WAF-D-20-0059.1](https://doi.org/10.1175/WAF-D-20-0059.1).
- do Carmo, M.P., 1992. Riemannian Geometry. Mathematics: Theory and Applications. 2 ed., Birkhäuser Boston, Cambridge, MA, USA.
- Dai, X., Lin, Z., Müller, H., 2021. Modeling sparse longitudinal data on Riemannian manifolds. *Biometrics* 77, 1328–1341. doi:[10.1111/biom.13385](https://doi.org/10.1111/biom.13385).
- Debavelaere, V., Durrleman, S., Allasonnière, S., 2020. Learning the clustering of longitudinal shape data sets into a mixture of independent or branching trajectories. *Int. J. Comput. Vis.* 128, 2794–2809. doi:[10.1007/s11263-020-01337-8](https://doi.org/10.1007/s11263-020-01337-8).
- Fishbaugh, J., Durrleman, S., Piven, J., Gerig, G., 2012. A framework for longitudinal data analysis via shape regression, in: *Medical Imaging 2012: Image Processing*, International Society for Optics and Photonics. SPIE. p. 83143K. doi:[10.1117/12.911721](https://doi.org/10.1117/12.911721).
- Fletcher, P.T., 2013. Geodesic regression and the theory of least squares on Riemannian manifolds. *Int. J. Comput. Vis.* 105, 171–185. doi:[10.1007/s11263-012-0591-y](https://doi.org/10.1007/s11263-012-0591-y).
- Fletcher, P.T., Lu, C., Pizer, S.M., Joshi, S., 2004. Principal geodesic analysis for the study of nonlinear statistics of shape. *IEEE Trans. Med. Imaging* 23, 995–1005. doi:[10.1109/TMI.2004.831793](https://doi.org/10.1109/TMI.2004.831793).
- Gousenbourger, P.Y., Massart, E., Absil, P.A., 2019. Data fitting on manifolds with composite Bézier-like curves and blended cubic splines. *Journal of Mathematical Imaging and Vision* 61, 645–671. doi:[10.1007/s10851-018-0865-2](https://doi.org/10.1007/s10851-018-0865-2).
- Gudmundsson, S., Kappos, E., 2002. On the geometry of tangent bundles. *Expo. Math.* 20, 1–41. doi:[10.1016/S0723-0869\(02\)80027-5](https://doi.org/10.1016/S0723-0869(02)80027-5).
- Hanik, M., Hege, H.C., Hennemuth, A., von Tycowicz, C., 2020. Nonlinear regression on manifolds for shape analysis using intrinsic Bézier splines, in: *Medical Image Computing and Computer Assisted Intervention – MICCAI 2020*, Springer. pp. 617–626. doi:[10.1007/978-3-030-59719-1\\_60](https://doi.org/10.1007/978-3-030-59719-1_60).
- Hanik, M., Hege, H.C., von Tycowicz, C., 2022. A nonlinear hierarchical model for longitudinal data on manifolds, in: *2022 IEEE 19th International Symposium on Biomedical Imaging (ISBI)*, pp. 1–5. doi:[10.1109/ISBI52829.2022.9761465](https://doi.org/10.1109/ISBI52829.2022.9761465).
- Hinkle, J.D., Fletcher, P.T., Joshi, S.C., 2014. Intrinsic polynomials for regression on Riemannian manifolds. *J. Math. Imaging Vis.* 50, 32–52. doi:[10.1007/s10851-013-0489-5](https://doi.org/10.1007/s10851-013-0489-5).
- Le Brigant, A., Arnaudon, M., Barbaresco, F., 2015. Reparameterization invariant metric on the space of curves, in: *International Conference on Geometric Science of Information*, Springer. pp. 140–149. doi:[10.1007/978-3-319-25040-3\\_16](https://doi.org/10.1007/978-3-319-25040-3_16).
- Machado, L.M., Silva Leite, F., 2007. Fitting smooth paths on Riemannian manifolds. *Int. J. Appl. Math. Stat.* 4, 25–53.
- Muralidharan, P., Fletcher, P.T., 2012. Sasaki metrics for analysis of longitudinal data on manifolds, in: *2012 IEEE Conference on Computer Vision and Pattern Recognition*, Providence, RI, USA, June 16–21, 2012, pp. 1027–1034. doi:[10.1109/CVPR.2012.6247780](https://doi.org/10.1109/CVPR.2012.6247780).

- Nava-Yazdani, E., Hanik, M., Ambellan, F., von Tycowicz, C., 2022a. On Gradient Formulas in an Algorithm for the Logarithm of the Sasaki Metric. Technical Report 22-12. ZIB.
- Nava-Yazdani, E., Hege, H.C., n, T.J.S., von Tycowicz, C., 2020. Geodesic analysis in kendall’s shape space with epidemiological applications. *Journal of Mathematical Imaging and Vision* 62, 549–559. doi:[10.1007/s10851-020-00945-w](https://doi.org/10.1007/s10851-020-00945-w).
- Nava-Yazdani, E., Hege, H.C., von Tycowicz, C., 2022b. A hierarchical geodesic model for longitudinal analysis on manifolds. *J. Math. Imaging Vis.* 64, 395–407. doi:[10.1007/s10851-022-01079-x](https://doi.org/10.1007/s10851-022-01079-x).
- Nava-Yazdani, E., Polthier, K., 2013. De Casteljau’s algorithm on manifolds. *Comput. Aided. Geom. Des.* 30, 722–732. doi:[10.1016/j.cagd.2013.06.002](https://doi.org/10.1016/j.cagd.2013.06.002).
- Niethammer, M., Huang, Y., Vialard, F.X., 2011. Geodesic regression for image time-series, in: *Medical Image Computing and Computer-Assisted Intervention – MICCAI 2011*, Springer. pp. 655–662. doi:[10.1007/978-3-642-23629-7\\_80](https://doi.org/10.1007/978-3-642-23629-7_80).
- Popiel, T., Noakes, L., 2007. Bézier curves and  $C^2$  interpolation in Riemannian manifolds. *J. Approx. Theory* 148, 111–127. doi:[10.1016/j.jat.2007.03.002](https://doi.org/10.1016/j.jat.2007.03.002).
- Postnikov, M.M., 2013. *Geometry VI: Riemannian Geometry*. Encyclopaedia of Mathematical Sciences, Springer, Berlin. doi:[10.1007/978-3-662-04433-9](https://doi.org/10.1007/978-3-662-04433-9).
- Rekabdarkolae, H.M., Krut, C., Fuentes, M., Reich, B.J., 2019. A bayesian multivariate functional model with spatially varying coefficient approach for modeling hurricane track data. *Spat. Stat.* 29, 351–365. doi:[10.1016/j.spasta.2018.12.006](https://doi.org/10.1016/j.spasta.2018.12.006).
- Rumpf, M., Wirth, B., 2015. Variational time discretization of geodesic calculus. *IMA J. Numer. Anal.* 35, 1011–1046. doi:[10.1093/imanum/dru027](https://doi.org/10.1093/imanum/dru027).
- Sasaki, S., 1962. On the differential geometry of tangent bundles of riemannian manifolds ii. *Tohoku Math. J. Second Ser.* 14, 146–155. doi:[10.2748/tmj/1178244169](https://doi.org/10.2748/tmj/1178244169).
- Schiratti, J.B., Allasonniere, S., Colliot, O., Durrleman, S., 2015. Learning spatiotemporal trajectories from manifold-valued longitudinal data. *Adv. Neural Inf. Process. Syst.* 28.
- Shao, L., Lin, Z., Yao, F., 2022. Intrinsic Riemannian functional data analysis for sparse longitudinal observations. *Ann. Stat.* 50, 1696–1721. doi:[10.1214/22-AOS2172](https://doi.org/10.1214/22-AOS2172).
- Snaiki, R., Snaiki, R., Wu, T., 2020. Revisiting hurricane track model for wind risk assessment. *Struct. Saf.* 87, 102003. doi:[10.1016/j.strusafe.2020.102003](https://doi.org/10.1016/j.strusafe.2020.102003).
- Su, J., Kurtek, S., Klasse, E., Srivastava, A., 2014. Statistical analysis of trajectories on Riemannian manifolds: Bird migration, hurricane tracking and video surveillance. *Ann. Appl. Stats.* 8, 530–552. doi:[10.1214/13-AOS701](https://doi.org/10.1214/13-AOS701).
- Su, Z., Klassen, E., Bauer, M., 2018. Comparing curves in homogeneous spaces. *Differ. Geom. Appl.* 60, 9–32. doi:[10.1016/j.difgeo.2018.05.001](https://doi.org/10.1016/j.difgeo.2018.05.001).
- Suparti, Santoso, R., Prahutama, A., Devi, A.R., Sudargo, 2019. Modeling longitudinal data based on Fourier regression. *J. Phys. Conf.* 1217, 012105. doi:[10.1088/1742-6596/1217/1/012105](https://doi.org/10.1088/1742-6596/1217/1/012105).
- Weinkle, J., Landsea, C., Collins, D., Musulin, R., Crompton, R.P., Klotzbach, P.J., Pielke, R., 2018. Normalized hurricane damage in the continental united states 1900–2017. *Nat. Sustain.* 1, 808–813. doi:[10.1038/s41893-018-0165-2](https://doi.org/10.1038/s41893-018-0165-2).